Remote Sensing Cloud Properties from High Spectral Resolution Infrared Observations

WILLIAM L. SMITH, XIA LIN MA, STEVEN A. ACKERMAN, H. E. REVERCOMB, AND R. O. KNUTESON

Cooperative Institute for Meteorological Satellite Studies, Space Science and Engineering Center, University of Wisconsin—Madison, Madison, Wisconsin

(Manuscript received 7 April 1992, in final form 28 August 1992)

ABSTRACT

A technique for estimating cloud radiative properties (i.e., spectral emissivity and reflectivity) in the infrared is developed based on observations at a spectral resolution of approximately 0.5 cm^{-1}. The algorithm makes use of spectral radiance observations and theoretical calculations of the infrared spectra for clear and cloudy conditions along with lidar-determined cloud-base and cloud-top pressure. An advantage of the high spectral resolution observations is that the absorption effects of atmospheric gases are minimized by analyzing between gaseous absorption lines. The technique is applicable to both ground-based and aircraft-based platforms and derives the effective particle size and associated cloud water content required to satisfy, theoretically, the observed cloud infrared spectra. The algorithm is tested using theoretical simulations and applied to observations made with the University of Wisconsin's ground-based and NASA ER-2 aircraft High-Resolution Infrared Spectrometer instruments.

1. Introduction

The 8–12-μm spectral window region is of major importance to the radiation budget and remote sensing of the earth–atmosphere system. The presence of clouds alters the incoming and outgoing radiation and modifies the atmospheric diabatic heating, thereby influencing the dynamics and climate of the atmosphere. Clouds also pose a problem in the interpretation of passive sounding measurements from meteorological satellites (Platt et al. 1973, 1980, 1981; Liou 1974; Stephens 1980; Wu 1984; Ackerman et al. 1990). The purpose of this work is to derive the longwave radiative properties of clouds in the atmospheric window region so that they can be parameterized as needed for incorporation in large-scale numerical models or for use in retrieval algorithms. In this investigation, the window region is referred to as the 800–1200-cm^{-1} (12.5–8.3 μm) spectral region. Within this wavenumber interval, absorption due to the atmospheric gases is relatively small, except for O_3. Absorption due to water vapor includes the selective absorption by weak lines and the continuous absorption by the water vapor continuum.

In this paper, we present an algorithm to derive the infrared (IR) radiative properties of clouds from high spectral resolution radiance observations. A multiple scattering model is introduced, which was used to develop and test the retrieval method. The technique is tested using theoretical radiance spectra and is applied to observations from the University of Wisconsin's ground-based and NASA ER-2 High-Resolution Infrared Spectrometer (HIS) instruments.

2. Cloud radiative property retrieval algorithm

The downwelling/upwelling spectral radiance is related to the cloud and atmospheric radiative and thermodynamic properties by the relations

$$R(\nu)\downarrow = \epsilon(\nu)B(\nu, T_c)\tau(\nu, P_c, P_s) + t(\nu)\tau(\nu, P_c, P_s)\int_0^{P_c} B(\nu, T)d\tau(\nu, P, P_c) + r(\nu)\tau(\nu, P_c, P_s)\left[B(\nu, T_s)\tau(\nu, P_s, P_c) + \int_{P_s}^{P_c} B(\nu, T)d\tau(\nu, P, P_c)\right] + \int_{P_c}^{P_s} B(\nu, t)d\tau(\nu, P, P_s) \quad (1)$$

for downwelling, and

$$R(\nu)\uparrow = \epsilon(\nu)B(\nu, T_c)\tau(\nu, P_0, 0) + t(\nu)\tau(\nu, P_c, 0)\left[B(\nu, T_s)\tau(\nu, P_s, P_c) + \int_{P_s}^{P_c} B(\nu, T)d\tau(\nu, P, P_c)\right] + r(\nu)\tau(\nu, P_c, 0)\int_0^{P_c} B(\nu, T)d\tau(\nu, P, P_c) + \int_{P_c}^{0} B(\nu, t)d\tau(\nu, P, 0) \quad (2)$$

Corresponding author address: Prof. William L. Smith, CIMSS, University of Wisconsin—Madison, 1225 West Dayton Street, Madison, WI 53706.

for upwelling. In the above equations ν is the wavenumber; $R(\nu)\downarrow$ and $R(\nu)\uparrow$ are the downwelling/upwelling spectral radiance at the surface/top of atmosphere; and $\epsilon(\nu)$, $t(\nu)$, and $r(\nu)$ are the cloud emissivity, transmissivity, and reflectivity, respectively; $B(\nu, T)$ is the Planck radiance corresponding to temperature T, P is atmospheric pressure, and $\tau(\nu, P_X, P)$ is the transmissivity of the atmosphere between the pressure level P_X and P. Subscripts c and s refer to the cloud and underlying ground surface conditions, respectively. The first term on the right of Eqs. (1) and (2) represent the emitted radiance contribution of an infinitesimally thin cloud. The second term indicates the transmitted radiance contribution from the atmosphere (and surface for the upwelling case) above/below clouds. The third term is the cloud reflected radiance contribution, and the last term represents the atmospheric contribution from below/above the clouds. Equations (1) and (2) assume that the clouds are infinitesimally thin. The clear-air radiance can be expressed as

$$R(\nu)^{\text{clr}}\downarrow = \int_0^{P_s} B(\nu, T)d\tau(\nu, P, P_s) \tag{3}$$

for downwelling and

$$R(\nu)^{\text{clr}}\uparrow = B(\nu, T_s)\tau(\nu, P_s, 0) + \int_{P_s}^{0} B(\nu, T)d\tau(\nu, P, 0) \tag{4}$$

for upwelling.

Subtracting (3) from (1) and (2) from (4) and using the relation $\epsilon(\nu) + r(\nu) + t(\nu) = 1$, the cloud spectral emissivities can be written as

$$\epsilon(\nu)\downarrow = \frac{\delta R(\nu)\downarrow - r(\nu)\tau(\nu, P_c, P_s)\left[B(\nu, T_s)\tau(\nu, P_s, P_c) + \int_{P_s}^{P_c} B(\nu, T)d\tau(\nu, P, P_c) - \int_0^{P_c} B(\nu, T)d\tau(\nu, P, P_c)\right]}{\tau(\nu, P_c, P_s)\left[B(\nu, T_c) - \int_0^{P_c} B(\nu, T)d\tau(\nu, P, P_c)\right]} \tag{5}$$

for downwelling, and

$$\epsilon(\nu)\uparrow = \frac{\delta R(\nu)\uparrow + r(\nu)\tau(\nu, P_c, 0)\left[\int_0^{P_c} B(\nu, T)d\tau(\nu, P, P_c) - \int_{P_s}^{P_c} B(\nu, T)d\tau(\nu, P, P_c) - B(\nu, T_s)\tau(\nu, P_s, P_c)\right]}{\tau(\nu, P_c, 0)\left[B(\nu, T_s)\tau(\nu, P_s, P_c) + \int_{P_s}^{P_c} B(\nu, T)d\tau(\nu, P, P_c) - B(\nu, T_c)\right]} \tag{6}$$

for upwelling, where $\delta R(\nu)\downarrow = R(\nu)\downarrow - R(\nu)^{\text{clr}}\downarrow$ for downwelling and $\delta R(\nu)\uparrow = R(\nu)^{\text{clr}}\uparrow - R(\nu)\uparrow$ for upwelling. While Eqs. (5) and (6) appear complex, they have distinct advantages when applied to high spectral resolution measurements in between absorption lines. For example, for the downward emissivity, $\epsilon(\nu)\downarrow$, the radiance above the cloud is small ($\int_0^{P_c} B(\nu, T)d\tau(\nu,P, P_c) \approx 0$) and the cloud reflectivity term is small [this term is generally more than one order of magnitude smaller than the cloud emission term in Eq. (1)], so that

$$\epsilon(\nu)\downarrow = \frac{\delta R(\nu)\downarrow}{\tau(\nu, P_c, P_s)B(\nu, T_c)}. \tag{7}$$

Between absorption lines, $\tau(\nu, P_c, P_s) \approx 1$; hence, to first order, $\epsilon(\nu)\downarrow$ is determined from an estimate of the clear-sky radiance spectrum and an effective cloud temperature. For the upwelling case, between absorption lines $\tau(\nu, P_c, 0) \approx 1$, so that Eq. (6) reduces to

$$\epsilon(\nu)\uparrow \approx \frac{\delta R(\nu)\uparrow - r(\nu)\left[\int_{P_s}^{P_c} B(\nu, T)d\tau(\nu, P, P_c) + B(\nu, T_s)\tau(\nu, P_s, \mathrm{P_c})\right]}{B(\nu, T_s)\tau(\nu, P_s, P_c) + \int_{P_s}^{P_c} B(\nu, T)d\tau(\nu, P, P_c) - B(\nu, T_c)}. \tag{8}$$

Derivation of $\epsilon(\nu)\uparrow$ is less straightforward than $\epsilon(\nu)\downarrow$. For high cirrus cloud between absorption lines, $R(\nu)^{\text{clr}}\uparrow \approx B(\nu, T_s)\tau(\nu, P_s, 0) + \int_{P_s}^{P_c} B(\nu, T)d\tau(\nu, P, P_c)$, since

$$\tau(\nu, P_c, 0) \approx 1.0.$$

$$\epsilon(\nu)\uparrow \approx \frac{[1 - r(\nu)]R(\nu)^{\text{clr}}\uparrow - R(\nu)\uparrow}{R(\nu)^{\text{clr}}\uparrow - B(\nu, T_c)}. \quad (9)$$

Thus, the $\epsilon(\nu)\uparrow$ is determined to first order from an estimate of the clear-sky radiance, cloud effective temperature, and the cloud reflectivity. In this paper, we present an iterative method to derive the cloud radiative properties for the window region using the complete radiative transfer relations, Eqs. (5) and (6). This cloud radiation property retrieval will hereafter be referred to as the CRPR algorithm.

3. Dataset

NASA ER-2-based High-Resolution Infrared Spectrometer (HIS) observations were used to specify the upwelling radiances for deriving the cloud radiometic properties. The HIS is a Michelson Interferometer developed primarily as a aircraft prototype of a new generation satellite sounder (Smith et al. 1986, 1987, 1990). It operates in the infrared region between 600 and 2600 cm^{-1} (16.8–3.8 μm) using three detectors to divide the entire spectrum into three bands: band 1 (600–1080 cm^{-1}), band 2 (1080–1850 cm^{-1}), and band 3 (2000–2600 cm^{-1}). The HIS spectra have a spectral resolving power ($\lambda/\delta\lambda$) of approximately 2000 providing a spectral resolution (apodized) of approximately 0.5 cm^{-1} for band 1, and 1.0 cm^{-1} for bands 2 and 3. The ground resolution of the HIS nadir observation is approximately 2 km from an ER-2 altitude of 19.8 km. A detailed description of the instrument and its calibration is given in Revercomb et al. (1988).

Observations of downwelling cloud radiances reported here were accomplished using a ground-based HIS system, which utilizes a BOMEM M-120 Interferometer produced commercially by BOMEM Incorporated, Quebec, Canada. The University of Wisconsin ground-based system utilizes three calibration sources to produce radiometrically accurate infrared radiation measurement in the range of 500–1667 cm^{-1} (20–6 μm) with a resolution of 1 cm^{-1} apodized. A more detailed discussion of the ground-based HIS M120 instrument is given by Knuteson et al. (1991).

In this study, cloud-base and cloud-top altitudes were assigned from lidar observations made simultaneously with the HIS spectra. In the case of the NASA ER-2-based observations, the lidar measurements of Spinhirne et al. (1988) were used. A description of the cloud aerosol lidar and its applications can be found in Spinhirne and Hart (1990). For deriving cloud-radiative properties from ground-based observations, base and top altitudes were based on measurements from the high spectral resolution lidar (Grund et al. 1990). Cloud-base and cloud-top temperature were obtained from temperature and moisture profiles measured simultaneously by radiosondes or by the NCAR Cross-Chain Loran Atmospheric Sounding System (CLASS), in combination with the lidar data. The observed atmospheric temperature and water vapor profiles were taken as input to FASCOD2 (See section 5) to yield the atmospheric clear-sky radiance spectra and transmittance profiles.

4. The multiple scattering model

To examine the feasibility of the CRPR algorithm for retrieving cloud radiative properties, a theoretical model is required to simulate observed radiances with known cloud and atmospheric properties. Assuming a plane-parallel horizontally homogeneous cloud, the IR radiative transfer equation is

$$\mu \frac{dI(\delta, \mu)}{d\delta} = I(\delta, \mu) - (1 - \omega_0)B(T) - \frac{\omega_0}{2}\int_{-1}^{1} P(\delta, \mu, \mu')I(\delta, \mu')d\mu', \quad (10)$$

where $I(\delta, \mu)$ is the azimuthally averaged monochromatic intensity, δ is the optical thickness, ω_0 is the single scattering albedo, $P(\delta, \mu, \mu')$ is the azimuthally averaged phase function, $B(T)$ represents the Planck function at temperature T, and $\mu = \cos(\theta)$ where θ is measured from the downward normal direction. An accurate technique to solve Eq. (10) is the doubling–adding method. This type of model has been discussed in detail in previous atmospheric studies (Grant and Hunt 1969; Wiscombe 1976; Wiscombe and Grams 1976; Wiscombe and Evans 1977; and Stephens 1978, 1980). It is assumed that the model cloud is composed of equivalent spherical ice particles (or water drops) distributed according to

$$n(r) = cr^{(1-3b)/b}\exp\left(\frac{-r}{ab}\right) \quad (11)$$

(Hansen 1971). In this formula $n(r)$ is the number density of particles in the range of effective radii r to $r + dr$, a is the effective radius (ratio of the third moment of the size distribution to the second moment), b is related to the dispersion, and c is a normalization constant that is associated with total particle concentration. For simplicity, the phase function used in Eq. (10) is the Henyen–Greenstein phase function

$$P(\mu^*) = \frac{1 - g^2}{(1 + g - 2g\mu^*)^{3/2}}, \quad (12)$$

where μ^* is the scatter angle (defined as the angle between the incident and scattered beams). The parameter g is the asymmetry factor for this phase function.

The asymmetry factor g together with the extinction coefficient σ_{ext} (used to define the optical thickness) and the single scattering albedo ω_0 are evaluated based on Mie scatter theory over the infrared spectral region with effective particle radii ranging from 5 to 30 μm. Figures 1 and 2 are samples of the single scattering parameters for ice particles of $a = 10$ μm and $b = 0.1$ and water drops of $a = 5$ μm and $b = 0.1$, respectively. Unlike the gaseous absorption, the single scattering properties are smoothly varying functions. Cloud radiative properties on absorption lines can therefore be derived from interpolation of properties derived from radiometric observations made between the absorption lines.

A plane-parallel model atmosphere consisting of three layers (cloud, above-cloud, and below-cloud layers) was employed to evaluate the transfer of thermal infrared radiation in a cloudy atmosphere. The atmospheric temperature and water vapor profiles were determined from the radiosonde/CLASS observations. Taking these radiosonde data as input to FASCOD2 (see section 5), the atmospheric clear-sky radiance spectra and transmittance profiles were simulated over the spectral region of interest, 800–1200 cm^{-1}. Table 1 lists the input data regarding the cloud model atmosphere (i.e., the cloud-base and cloud-top temperature, cloud height, and thickness).

Calculation of the transfer of infrared radiance through a cloudy atmosphere was carried out for 16 discrete emergent angles. The radiances emitted by the atmosphere below and above the cloud layer were generated from FASCOD2. In the computation of the cloud-layer radiance contribution, the effect of water vapor within clouds was taken into consideration by expressing the asymmetry parameter and the single scattering albedo of the cloud layer as

$$g' = \frac{g^*\delta_c + \delta_g}{\delta_c + \delta_g} \tag{13}$$

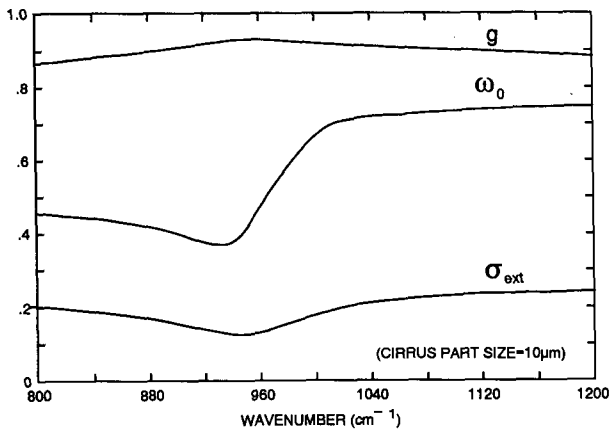

FIG. 1. Extinction coefficient, single scattering albedo, and asymmetry parameter spectra for ice particles of $a = 10$ μm and $b = 0.1$.

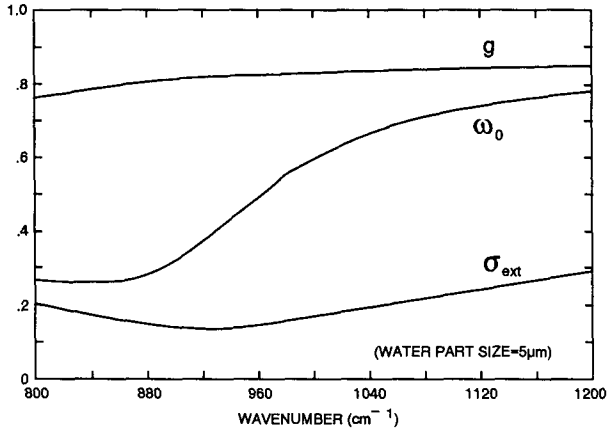

FIG. 2. As in Fig. 1 but for water drops of $a = 5$ μm and $b = 0.1$.

and

$$\omega_0' = \frac{\omega_0^* \delta_c}{\delta_c + \delta_g}, \tag{14}$$

where δ_c and δ_g represent cloud and gaseous optical thicknesses, respectively. In addition to simulating a cloud radiance spectrum, the multiple scattering model was also used to specify the beam emissivity and the beam reflectivity spectra of the cloud. Calculations were conducted for effective particle sizes ranging from 5 to 30 μm and ice/liquid water content (IWC/LWC) ranging from 0.0001 to 0.02 gm^{-3}. These calculations were used to construct lookup tables of cloud radiative properties. Each entry of the table consists of a cloud radiance, beam emissivity, and a beam reflectivity spectra as a function of a specified effective radius (r_e) and an IWC/LWC value.

5. Retrieval algorithm

Ground-based BOMEM and aircraft HIS radiance observations of clear and cloud spectral radiance together with lidar data and atmospheric profiles of temperature and water vapor were used to deduce the radiative properties of clouds.

Fast Atmospheric Signature Code 2 (FASCOD2) is a model for the accelerated line-by-line calculation of spectral transmittance and radiance for atmospheric problems (Clough et al. 1986). The program is applicable to spectral regions from the microwave to the near ultraviolet. In Eqs. (5) and (6), the atmospheric transmittance $\tau(\nu, P_s, P)$ [or $\tau(\nu, P_c, P)$] between the surface (or cloud) and pressure level P was calculated by FASCOD2 based on local atmospheric thermal structure and water vapor distribution. In Eqs. (13) and (14) the gaseous optical thickness δ_g is defined as $-\ln[\tau(\nu, P_1, P_2)]$, where τ is calculated from FASCOD2.

The surface radiative contribution plays an important role in the downlooking observations. An incorrect

TABLE 1. Cloud model data specified for cirrus and water clouds.

Date of observation	Cloud type	Interferometer	Time (UTC)	T_{top} (K)	T_{base} (K)	H_{top} (km)	H_{base} (km)	Thickness (km)
1 December 1989	Cirrus	Synthetic BOMEM	2124	215.86	244.78	10	6	4
2 November 1986	Cirrus	Synthetic HIS	2000	215.69	233.08	10	8	2
5 December 1989	Water	Synthetic BOMEM	1950	270.15	275.61	2	1.5	0.5
2 November 1986	Water	Synthetic HIS	1800	269.17	270.07	2	1.5	0.5

estimation of the surface temperature would introduce differences between the upwelling radiance spectrum and that calculated by FASCOD2. In order to alleviate this potential source of error, HIS "window" channel radiances observed for clear atmospheric conditions are used to estimate the surface radiative contribution. The atmospheric radiation calculations are carried out for different "effective" surface skin temperatures assuming unity surface emissivity. (The "effective" temperature is the inverse Planck function of the product of surface emissivity and the Planck radiance corresponding to the true surface skin temperature.) A particular "effective" surface skin temperature is chosen as the value that minimizes the difference between the calculated and measured clear-sky radiances for the "windows" between absorption lines. The spectrum of surface radiance is then defined as the Planck radiance corresponding to the spectrum of surface "effective" brightness temperature obtained by interpolation between the windows within the spectrum. It is noted that this method accounts for the surface emissivity in an implicit manner and avoids the problem of defining the true physical temperature of the surface skin.

a. Gamma technique

Residual differences exist between the observed downwelling (upwelling) radiance spectrum and that calculated using the FASCOD2 line-by-line program with atmospheric state data from in situ measurements (Revercomb et al. 1990). These discrepancies are due to uncertainties in the atmospheric state parameters (particularly water vapor and ozone) and to errors in the spectroscopic data (i.e. line strengths and shapes). As a result, it is necessary to make an adjustment to the atmospheric transmittance in order to minimize the differences between the observed radiance and the FASCOD2 calculated radiance. The adjustments were made to the transmittance profiles assuming that

$$\tau^*(\nu, P_l, P) = [\tau(\nu, P_l, P)]^{\gamma(\nu)}, \qquad (15)$$

where $\gamma(\nu)$ is the adjustment factor, $\tau(\nu, P_l, P)$ is the nonadjusted transmittance, and $\tau^*(\nu, P_l, P)$ is the adjusted transmittance; l represents the surface or cloud-top (or base) level. The adjustment factor is determined by the following iterative formula:

$$\gamma_n(\nu) = \gamma_{n-1}(\nu) + \frac{\partial\gamma_{n-1}(\nu)}{\partial R_c(\nu)}[R_m(\nu) - R_c(\gamma_{n-1})] \qquad (16)$$

and

$$\frac{\partial\gamma_{n-1}(\nu)}{\partial R_c(\nu)} = \frac{\gamma_{n-1}(\nu) - \gamma_{n-2}(\nu)}{R_c(\gamma_{n-1}) - R_c(\gamma_{n-2})}, \quad n \geq 2, \qquad (17)$$

where $R_m(\nu)$ is the measured clear radiance and $R_c(\nu)$ is the radiance calculated using the adjusted atmospheric transmittance profiles. The initial γ value was assigned to be 0.95 or 1.05 depending on the difference between $R_m(\nu)$ and $R_c(\nu)$ (using the original atmospheric transmittance profiles). The iteration is executed until $|\gamma_n(\nu) - \gamma_{n-1}(\nu)| \leq 0.01$. Figure 3 shows measured (curve A) and FASCOD2 calculated (curve B) radiance spectra before application of the Gamma technique. Obviously, after the adjustments were made, the calculated radiance is coincident with the measured clear radiance. Figure 4 shows the γ spectrum that produces agreement between the observed and calculated radiances.

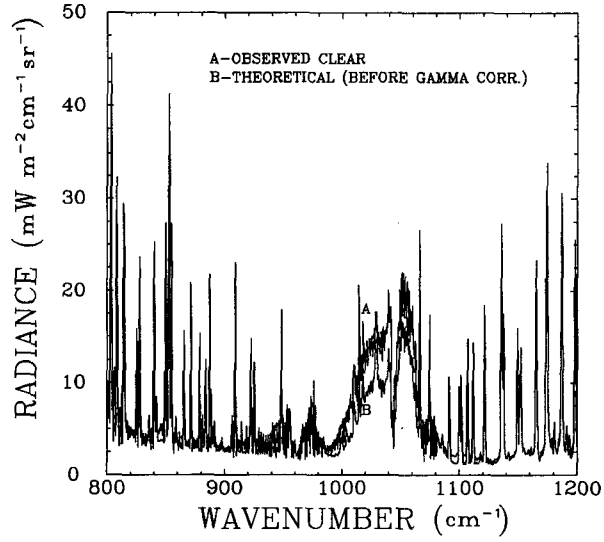

FIG. 3. FASCOD2 calculated and measured radiance spectra.

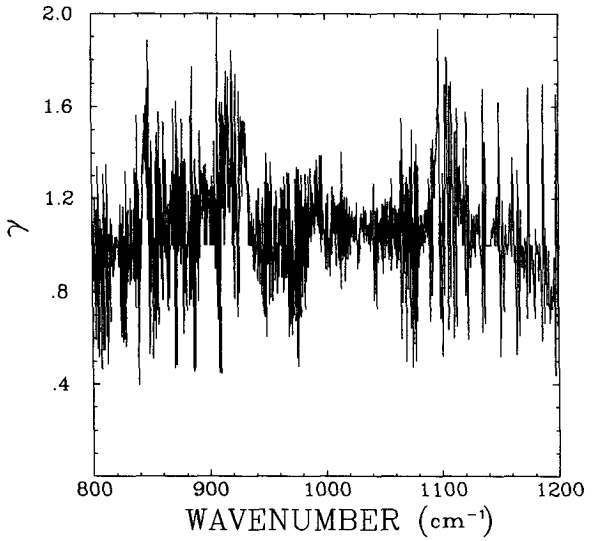

FIG. 4. Gamma spectrum.

b. *Initial and RTE adjusted emissivities*

Assuming a cloud reflectivity of zero, the initial emissivity of the cloud is calculated from Eqs. (5) or (6) using clear and cloudy radiance measurements and the atmospheric transmittance profiles. The cloud-free observation periods are determined from lidar measurements. Within this period, a radiance spectrum with lowest (highest) values for downwelling (upwelling) radiance is selected as the clear radiance measurement. As discussed below, the cloud reflectivity is taken into consideration using theoretical calculations to derive a new "corrected" emissivity. This corrected emissivity is referred to as the RTE (Radiative Transfer Equation) adjusted emissivity.

The effective particle size of clouds plays a major role in determining the shape of the cloud emissivity spectrum. Therefore, a particular cloud particle size is chosen to minimize the absolute differences of the ratio of the retrieved emissivity, ϵ_R to the theoretical emissivity, ϵ_T, from the spectral mean wavenumber ratio value. That is

$$\min \sum_{i=1}^{20} \left| \frac{\epsilon_R(\nu_i)}{\epsilon_T(\nu_i)} - \bar{\epsilon} \right|, \qquad (18)$$

where

$$\bar{\epsilon} = \frac{1}{20} \sum_{i=1}^{20} \frac{\epsilon_R(\nu_i)}{\epsilon_T(\nu_i)}$$

at the 20 spectral regions ν_i, indicated by triangles in Fig. 5a (constrained to be off any water vapor absorption lines within the 800–1200-cm^{-1} window region). Here ϵ_T represents the theoretical emissivities derived from the FASCOD2 and multiple scattering model calculations and retrieved from the theoretical look-up tables according to predetermined particle size and water content representing different types of clouds; ϵ_R is derived using Eq. (5) or (6) where the cloud spectral reflectivity is that associated with ϵ_T. Based on the retrieved particle size, the absolute differences

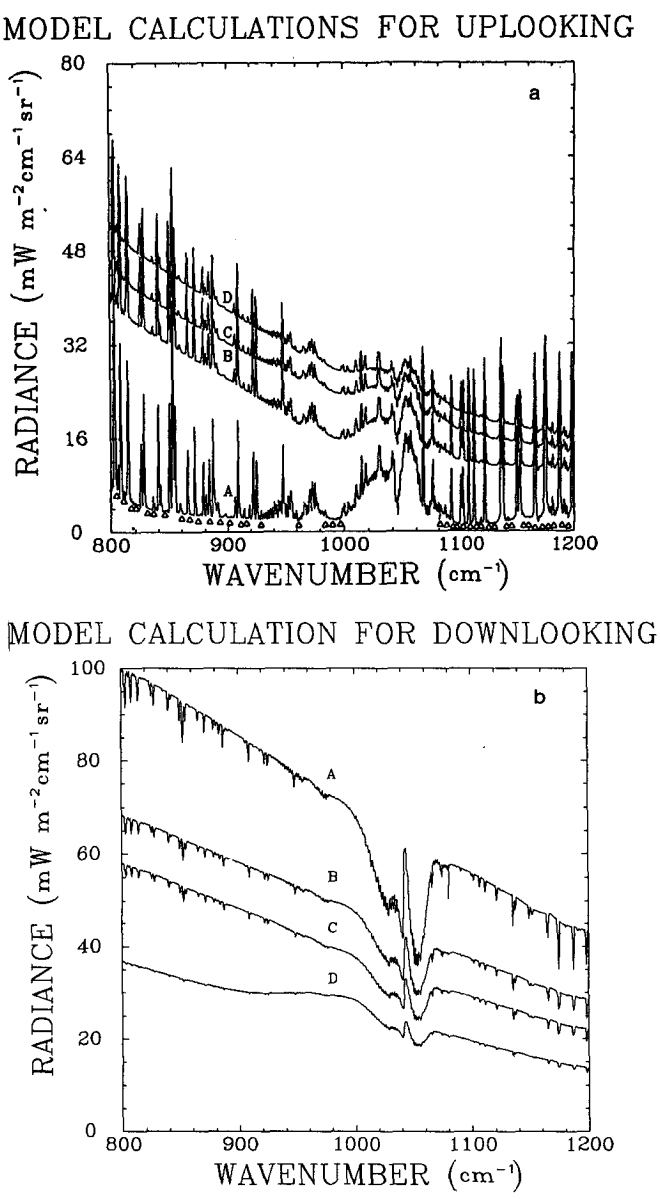

FIG. 5. Cirrus cloud synthetic radiance spectra. Cloud information is taken from Table 1. (a) Ground-based simulation: the curve "A" is clear radiance, "B" cloudy radiance with particle size = 10 μm and IWC = 0.0030, "C" cloudy radiance with particle size = 20 μm and IWC = 0.0098, and "D" cloudy radiance with particle size = 15 μm and IWC = 0.0122. (b) ER-2-based simulation: the curve "A" is clear radiance, "B" cloudy radiance with particle size = 20 μm and IWC = 0.0066, "C" cloudy radiance with particle size = 30 μm and IWC = 0.0162, and "D" cloudy radiance with particle size = 10 μm and IWC = 0.0122.

$$\sum_{i=1}^{20} |\epsilon_R(\nu_i) - \epsilon_T(\nu_i)|$$

are then calculated at the same 20 spectral intervals after varying the cloud water content. A water content value that produces the minimum difference is then chosen as the correct one.

To summarize, the four steps to derive the RTE-adjusted emissivity are

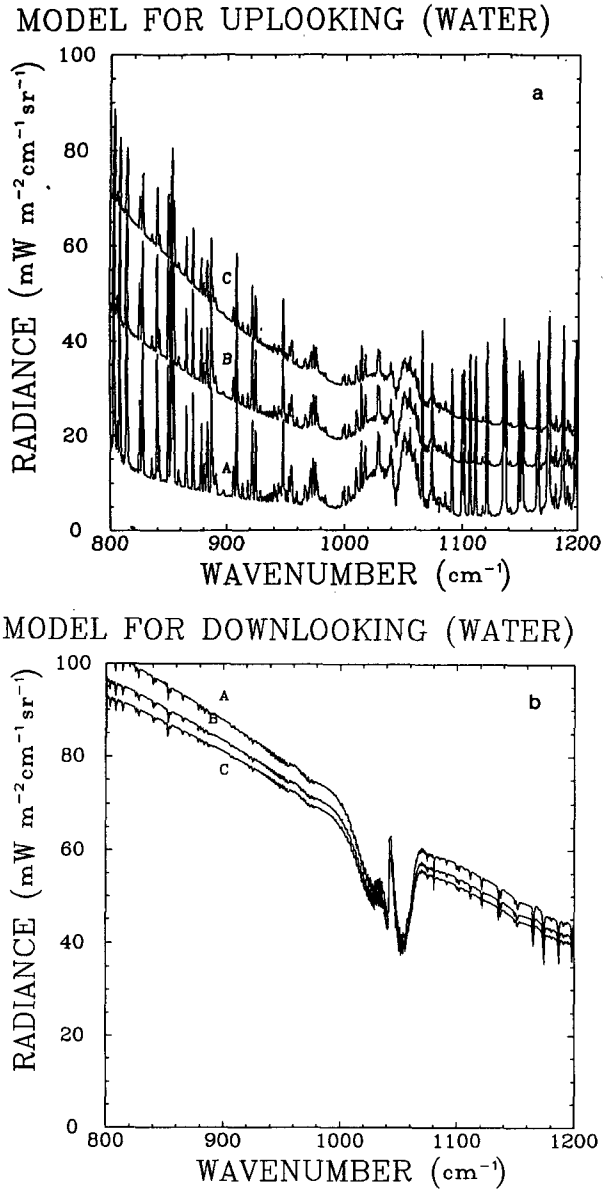

FIG. 6. Water cloud synthetic radiance spectra. Cloud information is taken from Table 1. (a) Ground-based simulation: the curve "A" is clear radiance, "B" cloudy radiance with particle size = 7.5 μm and LWC = 0.0082, and "C" cloudy radiance with particle size = 5 μm and LWC = 0.0146. (b) ER-2-based simulation: the curve "A" is clear radiance, "B" cloudy radiance with particle size = 7.5 μm and LWC = 0.0070, and "C" cloudy radiance with particle size = 5 μm and LWC = 0.0098.

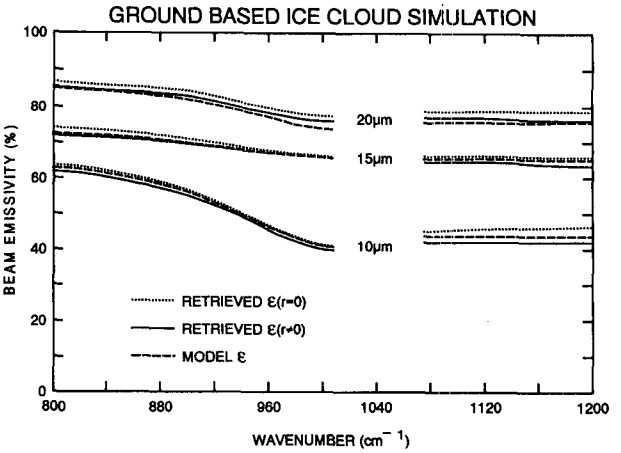

FIG. 7. Cirrus cloud emissivity spectra from ground-based simulation.

i) An initial emissivity spectrum is derived from Eq. (5) or (6) assuming no cloud reflectivity and an effective cloud temperature determined from a lidar cloud altitude and a temperature–altitude profile.

ii) Based on a lookup table derived from theoretical calculations, an effective particle size is chosen that achieves the minimization given by Eq. (18).

iii) A cloud water content is chosen based on the minimization defined by Eq. (19).

iv) The final ϵ_R is derived from Eqs. (5) or (6) where the cloud reflectivity is defined from the lookup table according to predetermined effective particle size and water content in steps (ii) and (iii).

6. Results and discussion

a. Synthetic radiance test

The technique described in section 5 was used to derive the IR radiative properties of cirrus and liquid

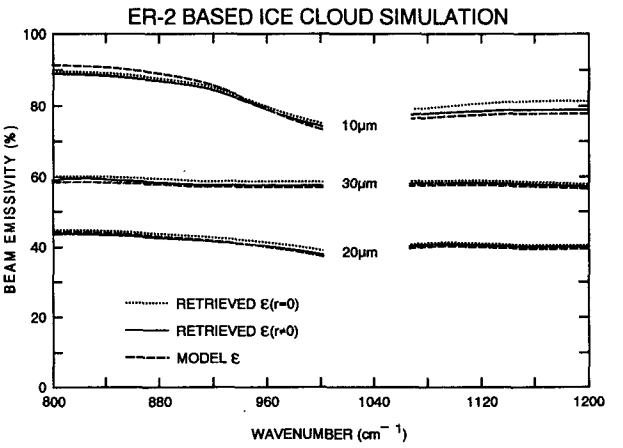

FIG. 8. As in Fig. 7 but from ER-2-based simulation.

TABLE 2. The retrieved cirrus and water cloud effective particle size and water content from synthetic ground-based uplooking (BOMEM) and ER-2 aircraft downlooking (HIS) spectral radiance observations.

Date of observation	Cloud type	Interferometer	Particle size (μm) True	Particle size (μm) Ret	Ice or liquid water content (g m^{-3}) True	Ice or liquid water content (g m^{-3}) Ret
1 December 1989	Cirrus	Synthetic BOMEM	10	10	0.0030	0.0021
			15	15	0.0122	0.0066
			20	20	0.0098	0.0062
2 November 1986	Cirrus	Synthetic HIS	10	10	0.0122	0.0102
			20	20	0.0066	0.0058
			30	30	0.0162	0.0142
5 December 1989	Water	Synthetic BOMEM	5	5	0.0146	0.0138
			7.5	7.5	0.0082	0.0078
2 November 1986	Water	Synthetic HIS	5	5	0.0098	0.0060
			7.5	7.5	0.0070	0.0062

water clouds from synthetic ground-based and aircraft-based radiance observations generated by the multiple scattering model. Figures 5a,b show the clear and cirrus cloud radiance spectra calculated with the theoretical model over the 8–12-μm window region for uplooking BOMEM and downlooking HIS simulation, respectively. Similar results are presented in Figs. 6a,b for liquid water clouds. The cloud-layer information used in the synthetic radiance calculations is listed in Table 1. As can be seen from these figures, the emission by the water vapor lines is more evident in the uplooking cases because of the very low radiance background (i.e., deep space or cold clouds) to the relatively warm water vapor.

Figures 7 and 8 display cirrus cloud beam emissivity spectra over the same spectral region for uplooking and downlooking cases, respectively. The dashed line represents the theoretical emissivity, the solid line represents RTE-adjusted emissivity, and the dotted line represents the initial emissivity retrieval assuming zero reflectivity. A comparison of the initial and RTE-adjusted spectra reveals a close agreement between both the shapes of the emissivity curves and also the emissivity values. Note that the beam reflectance in these cases is small, less than 5%. A number of important features emerge from these computations. First, the slope of the emissivity curve in the 800–1200-cm^{-1} region is, to a considerable degree, dependent on the effective cloud particle size. The slope of the curve becomes steeper with smaller cloud effective particle sizes. For a specified cloud thickness, the cloud emissivity depends basically upon the water content, the particle size, and the temperature of the cloud. For uplooking

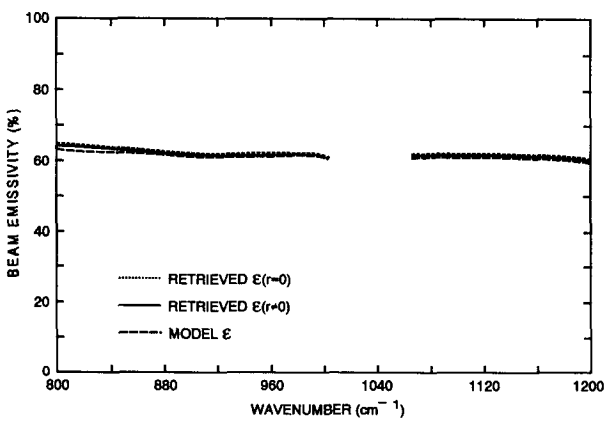

FIG. 9. Cirrus cloud emissivity spectra from ER-2-based simulation but using midcloud T = 224.4 K, the retrieved particle size = 30 μm, and IWC = 0.0158.

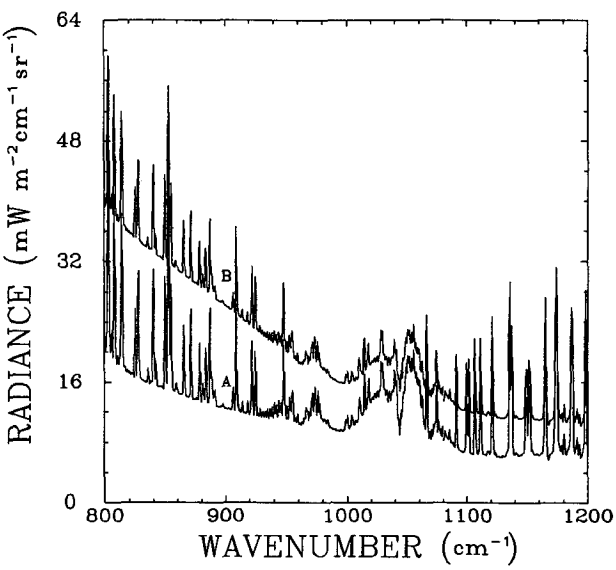

FIG. 10. Simulation of ground-based measurement of cirrus cloud radiance: "A" is synthetic with particle size = 30 LWC = 0.0030; "B" is the same as "A" but with particle size = 10.

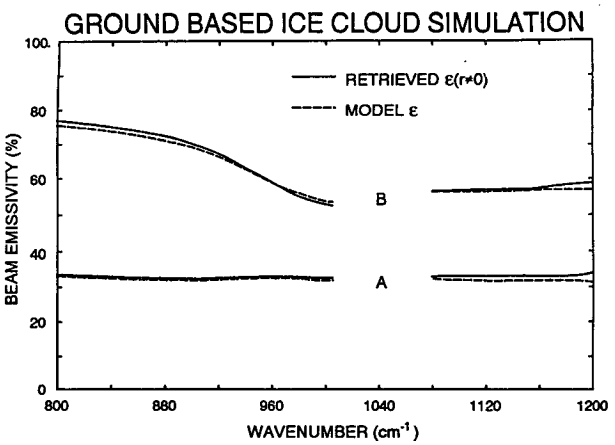

FIG. 11. Cirrus cloud emissivity spectra derived from simulated ground-based measured radiance spectrum using a midcloud temperature. Curves A: model particle size = 30 and IWC = 0.0030; retrieved particle size = 30 and IWC = 0.0032. Curves B: model particle size = 10 and IWC = 0.0030; retrieved particle size = 10, and IWC = 0.0030.

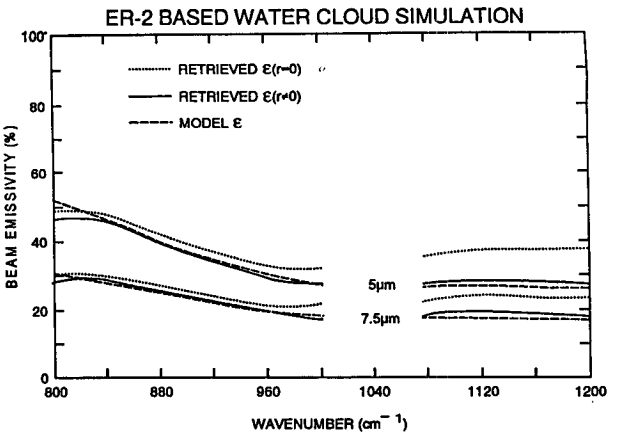

FIG. 13. As in Fig. 12 but from ER-2-based simulation.

emissivity calculations, the cloud-base temperature was used; for downlooking emissivity calculations, the cloud-top temperature was used. While the cloud temperature is fixed, the ice or liquid water content of the cloud greatly affects the optical depth and so has a significant effect on the derived IR radiative properties. As seen in Figs. 7 and 8, differences between adjusted and theoretical emissivities are small. Finally, the variation in the calculated emissivity spectrum from one synthetic cloudy radiance spectrum to another reflects the different radiative properties of clouds. Therefore, it would offer a simple way to retrieve cloud effective particle size and water content. Table 2 lists the model and retrieved cloud effective particle sizes and ice or liquid water contents. It can be seen that the retrieved cloud effective particle size is the same as the true model

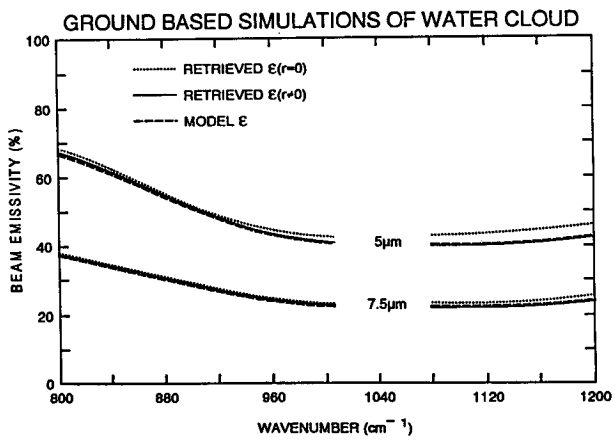

FIG. 12. Water cloud emissivity spectra from ground-based simulation. See Table 2 for explanation of conditions.

one (i.e., the one used to "synthesize" the observations), while the retrieved ice or liquid water content is always smaller than the true value, owing to the choice of assigning cloud-base or cloud-top temperature. Figure 9 shows a beam emissivity spectrum calculated for the 30-μm particle size case shown in Fig. 8 but using a midcloud temperature rather than the cloud-top temperature. The two-beam emissivity spectrum has a slightly larger magnitude, and consequently the retrieved IWC is slightly larger using a midcloud temperature rather than the cloud-top temperature.

Figure 10 shows the downwelling cirrus cloud radiance spectra reaching the surface as calculated for different effective particle sizes but for the same total ice water content. This calculation clearly demonstrates that the spectral variation of the downwelling radiance depends not only on ice water content but also on effective particle size. Figure 11 displays cirrus cloud beam emissivity spectra calculated using CRPR technique with the radiance spectra shown in Fig. 10. As can be seen, a good agreement between the retrieved emissivity spectrum (solid line) and the actual emissivity spectrum (dashed line) is achieved. Thus, the spectral independence of the radiance sensitivities to the effective particle size and ice water content is large enough for an unambiguous retrieval of both cloud properties.

A similar emissivity calculation was carried out for water cloud cases. The clear and cloudy radiance spectra displayed in Fig. 6 over the 800–1200-cm^{-1} region were used for emissivity derivations. Figures 12 and 13 illustrate the water cloud emissivity spectra from different synthetic radiances for both uplooking (BOMEM) and downlooking (HIS) cases, respectively. The symbols used in these figures are the same as in Fig. 7. The retrieved emissivity spectrum is in excellent agreement with the true emissivity spectrum. As noted previously, a comparison of the true and retrieved cloud microphysical properties is shown in Table 2.

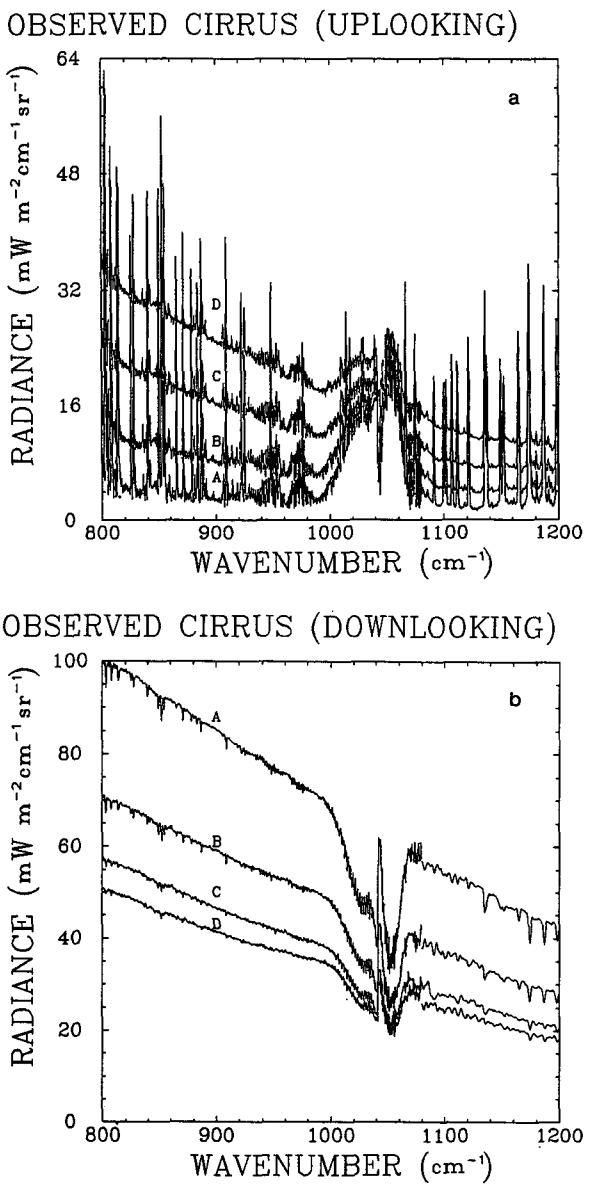

FIG. 14. Clear and cirrus cloud radiance spectra. (a) Ground-based BOMEM observations: the curve "A" is clear radiance; curves "B", "C", "D" denote cloudy radiances at different observation times on 1 Dec 1989. (b) ER-2 HIS observations: the curve "A" is clear radiance; curves "B", "C", and "D" denote cloudy radiances at the different observation times on 2 Nov 1986.

b. *Application to observations*

The technique for deriving IR radiative properties was applied to observations of cirrus and water clouds made from ground-based BOMEM and NASA ER-2-based High-Resolution Infrared Spectrometer (HIS) instrument. The Gamma technique described in section 5a was used in FASCOD2-calculated atmospheric transmittance in order to minimize differences between observed clear-air radiance and FASCOD2-calculated

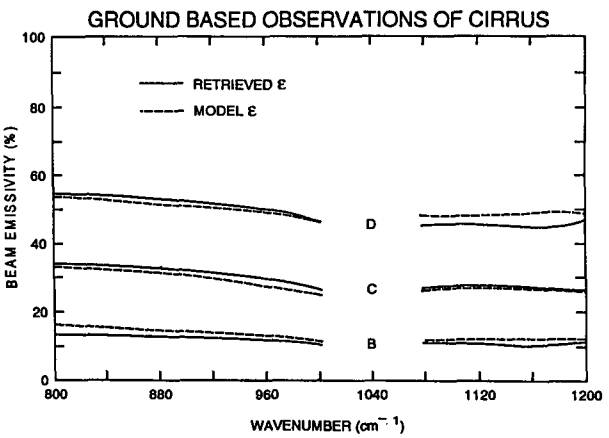

FIG. 15. Cirrus cloud emissivity spectra derived from ground-based BOMEM observations.

radiance. Lidar and radiosonde observations simultaneous to the radiance observations were collected. Figures 14a and 14b show examples of clear and cirrus cloud radiance spectra observed for the spectral region 800–1200 cm^{-1} uplooking and downlooking situations. Curve A is a clear spectrum; the other three curves are cloudy spectra observed at different times. Figures 15 and 16 illustrate cirrus cloud emissivity spectra retrieved using the CRPR technique with the clear and cloudy radiance observations. (The initial retrieved emissivity spectrum does not appear in these figures because of its good agreement with the final retrieved spectrum due to the very small reflectivity of cirrus cloud.). As a result of the minimization procedure used in the retrieval process, the RTE-adjusted emissivity spectrum closely matches the "theoretical" emissivity spectrum corresponding to the retrieved microphysical cloud properties.

Observations made for several liquid water cloud examples are depicted in Figs. 17a and 17b. Emissivity

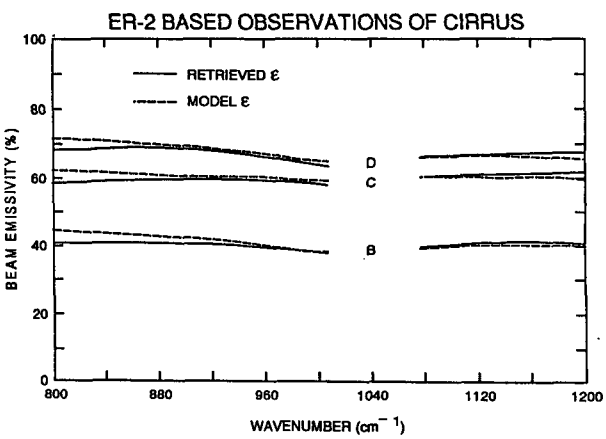

FIG. 16. As in Fig. 15 but derived from ER-2-based HIS observations.

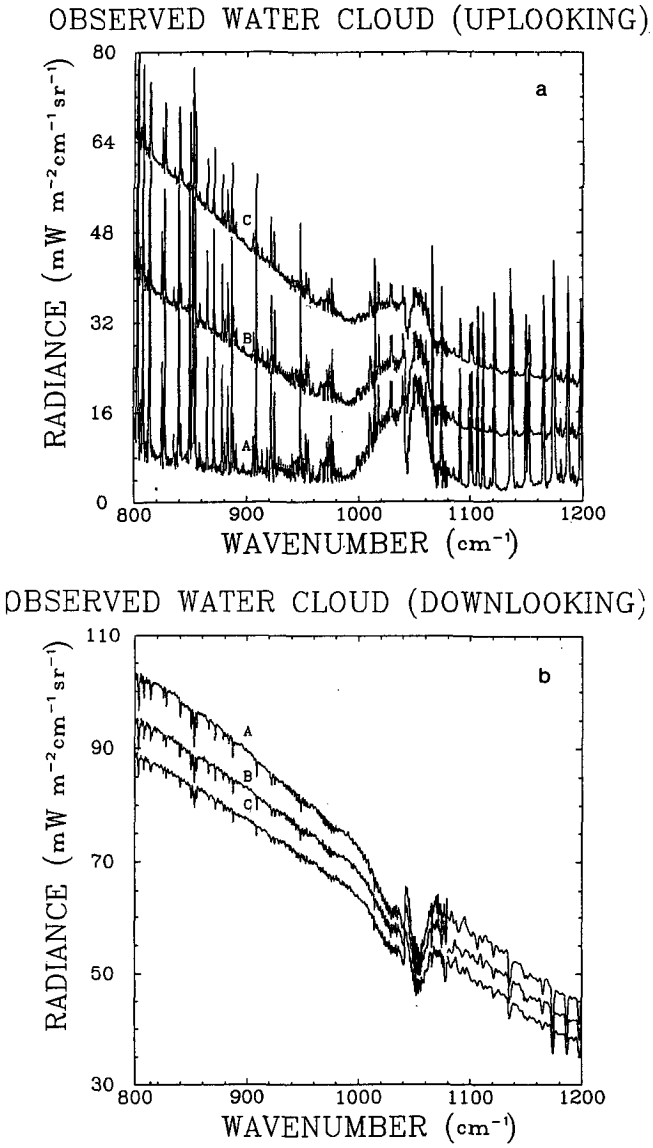

FIG. 17. Clear and water cloud radiance spectra. (a) Ground-based BOMEM observations: the curve "A" is clear radiance; curves "B" and "C" denote cloudy radiances at the different observation time on 5 Dec 1989. (b) ER-2 based HIS observations: the curve "A" is clear radiance; curves "B" and "C" denote cloudy radiances at the different observation times on 2 Nov 1986.

spectrum retrievals were made from these observations. Figures 18 and 19 present water cloud emissivity spectra retrieved and calculated from retrieved cloud properties. Table 3 lists observed cirrus and water cloud geometric properties and the retrieved cloud effective particle size and water content. Generally speaking, there is good agreement between the initial retrieved emissivity spectrum and the final retrieved emissivity spectrum for the 800–1000-cm^{-1} region, indicating that cloud reflection does not have a significant impact on the cloud emissivity retrieval for either uplooking or

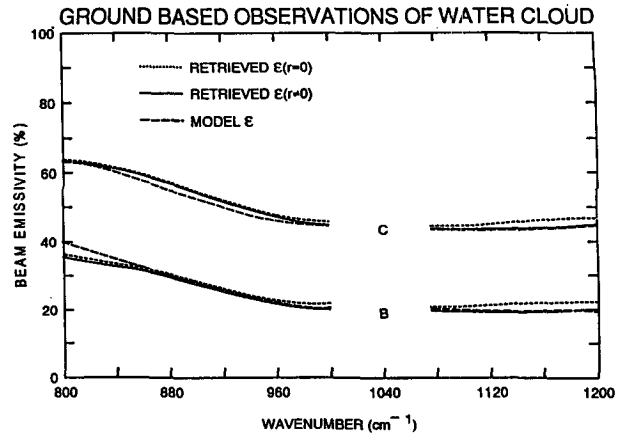

FIG. 18. Water cloud emissivity spectra derived from ground-based BOMEM observations.

downlooking observations. This result could greatly simplify the CRPR technique for inferring cloud radiative properties. However, as shown in Figs. 13 and 19, the influence of cloud reflection must be taken into consideration for the clouds with small effective particle size and large water content. Moreover, the CRPR technique yields retrievals of an effective particle size and water content that are theoretically consistent with the retrieved emissivity spectrum.

7. Conclusions

This study presents a new technique for inferring water and cirrus cloud radiative and microphysical properties. The technique was tested using theoretical calculations and applied to observations made from ground-based BOMEM and NASA high-altitude ER-2 aircraft-based HIS instruments made in conjunction with lidar cloud backscatter and in situ atmospheric temperature and moisture measurements. The re-

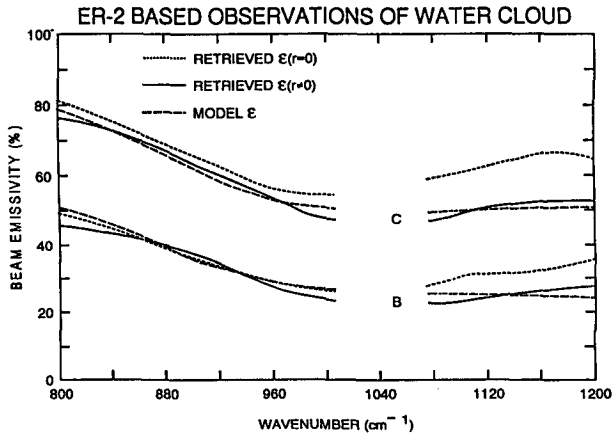

FIG. 19. As in Fig. 18 but from ER-2 based HIS observations.

TABLE 3. The cirrus and water cloud effective particle size and water content retrieved from actual ground-based uplooking (BOMEM) and aircraft downlooking (HIS) spectral radiance observations.

Date of observation	Time (UTC)	Cloud type	Interferometer	T_{top} or T_{base} (K)	H_{top} or H_{base} (km)	Thickness (km)	Particle size Ret (μm)	Ice or liquid water content Ret (g m^{-3})
1 December 1989	2337	Cirrus	Observations BOMEM	243.86	6.3	1.0	20	0.0038
	2229			243.86	6.3	2.3	15	0.0014
	2125			243.86	6.3	3.0	15	0.0006
2 November 1986	2036	Cirrus	Observations HIS	215.69	10.0	1.0	20	0.0122
	2035			215.69	10.0	1.0	25	0.0126
	2034			215.69	10.0	1.0	20	0.0058
5 December 1989	2237	Water	Observations BOMEM	275.61	1.5	0.5	7.5	0.0170
	2224			275.61	1.5	0.5	5	0.0062
2 November 1986	1633	Water	Observations HIS	270.07	2.0	0.5	5	0.0186
	1631			270.07	2.0	0.5	5	0.0078

trieved emissivity spectrum is in good agreement with the true theoretical spectrum obtained by calculation with a multiple scattering model.

This technique not only retrieves cloud IR radiative properties but also, under the assumption of cloud homogeneity, yields the cloud microphysical properties (e.g., cloud effective particle size and water content) that are theoretically consistent with the retrieved radiative properties. These cloud microphysical quantities are extremely useful for radiative budget studies, and to develop parameterizations of cloud radiative properties in climate and weather dynamic models (Stephens et al. 1990). The retrieved (effective) IWC or LWC will differ from the actual contents dependent upon 1) the choice of cloud effective temperature, 2) the assumption of equivalent spherical ice particles, and 3) the inhomogeneity of the cloud's microphysical properties. Further investigation is needed to estimate the impact of these assumptions on the utility and accuracy of the derived radiative properties.

The results of numerous tests (not shown here) illustrate that the influence of cloud reflection is not serious for nadir viewing within the 800–1200-cm^{-1} spectral region for either downwelling or upwelling radiance observations. Thus, the initial emissivity spectrum retrieved solely from the radiance observations can be used for many applications (e.g., profile retrieval). This greatly simplifies the application of the CRPR technique for remote sensing of cloud properties. For the retrieval of radiative effective cloud particle size and LWC or IWC, the full CRPR technique is required.

Finally, this study depicts the spectral variability of cloud optical properties within the window region (Ackerman et al. 1990). As clearly demonstrated, neither cirrus nor water clouds can be assumed to be blackbody or graybody emitters for climate studies or for the interpretation of satellite radiative measurements.

Acknowledgments. This research was funded by the National Aeronautics and Space Administration under Grant NAG-1-1177 and the Department of Energy under Grant DE-FG02-90GR61057. The authors gratefully acknowledge the contributions of H. B. Howell and H. M. Woolf of NOAA/NESDIS at the University of Wisconsin for their assistance with the development of the software required for the calculations presented here.

REFERENCES

Ackerman, S. A., W. L. Smith, J. D. Spinhirne, and H. E. Revercomb, 1990: The 27–28 October 1986 FIRE IFO cirrus case study: Spectral properties of cirrus clouds in the 8–12-μm window. *Mon. Wea. Rev.*, **118,** 2377–2388.

Clough, S. A., F. X. Kneizys, E. P. Shettle, and G. P. Anderson, 1986: Atmospheric Radiation and Transmittance: FASCOD2. *Proc. Sixth Conf. on Atmospheric Radiation,* Williamsburg, Amer. Meteor. Soc., 141–144.

Grant, I. P., and G. Hunt, 1969: Discrete space theory of radiative transfer I fundamentals. *Proc. Roy. Soc. London,* **A313,** 183–197.

Grund, C. J., E. W. Eloranta, D. P. Wylie, and H. E. Revercomb, 1990: Lidar and radiometric observation of local and mesoscale cirrus cloud properties with high spectral and spatial resolution. *15th Int. Laser Radar Conf. 1990,* Tomsk, USSR, Opt. Soc. Amer., 324–332.

Hansen, J. E., 1971: Multiple scattering of polarized light in a planetary atmosphere. Part II: Sunlight reflected by terrestrial water clouds. *J. Atmos. Sci.,* **28,** 1400–1426.

Knuteson, R. O., H. E. Revercomb, W. L. Smith, H. Buijs, R. Dedecker, H. B. Howell, H. M. Woolf, S. A. Ackerman, 1991: Realization of A low-cost ground-based temperature, humidity, and trace gas profiling system. *Seventh Symp. on Meteorological Observations and Instrumentation,* New Orleans, Amer. Meteor. Soc., J73–J74.

Liou, K. N., 1974: On the radiative properties of cirrus in the window region and their influence on remote sensing of the atmosphere. *J. Atmos. Sci.,* **31,** 522–532.

Platt, C. M. R., 1973: Lidar and radiometric observations of cirrus clouds. *J. Atmos. Sci.,* **30,** 1191–1204.

——, and G. L. Stephens, 1980: The interpretation of remotely sensed high cloud emittances. *J. Atmos. Sci.,* **37,** 2314–2322.

——, and A. C. Dilley, 1981: Remote sounding of high clouds. IV: Observed temperature variations in cirrus optical properties. *J. Atmos. Sci.,* **38,** 1069–1082.

Revercomb, H. E., H. Buijs, H. B. Howell, D. D. Laporte, W. L. Smith, and L. A. Sromovsky, 1988: Radiometric calibration of IR Fourier transform spectrometers: Solution to a problem with

the High-Spectral Resolution Interferometer Sounder. *Appl. Optics,* **27,** 3210–3218.

——, R. O. Knuteson, W. L. Smith, H. M. Woolf, and H. B. Howell, 1990: Spectroscopic inferences from HIS measurements of atmospheric thermal emission. Optical remote sensing of the atmosphere, 1990. *Tech. Dig.,* **4.**

Smith, W. L., H. E. Revercomb, H. B. Howell, H. M. Woolf, and D. D. Laporte, 1986: The High Resolution Interferometer Sounder (HIS). CIMSS View. Vol II. University of Wisconsin.

——, H. B. Howell, H.-L. Huang, and H. E. Revercomb, 1987: The simultaneous retrieval of atmospheric temperature and water vapor profiles-Applications to measurements with the high spectral resolution interferometer sounder (HIS). *RSRM 87, Advances in Remote Sensing Retrieval Methods,* Deepak 189–202.

——, H. E. Revercomb, H. B. Howell, H.-L. Huang, R. O. Knuteson, E. W. Koenig, D. D. LaPorte, S. Silverman, L. A. Sromovsky, and H. M. Woolf, 1990: GHIS-The GOES High Resolution Interferometer Sounder. *J. Appl. Meteor.,* **29,** 1189–1224.

Spinhirne, J. D., and W. D. Hart, 1990: Cirrus structure and radiative parameters from airborne lidar and spectral radiometer observations: The 28 October 1986 FIRE study. *Mon. Wea. Rev.,* **118,** 2329–2343.

——, D. L. Hlavka, and W. D. Hart, 1988: ER-2 lidar observations from the October 1986 FIRE Cirrus Experiment. NASA Tech. Memo., 100704.

Stephens, G. L., 1978: Radiative properties of extended water clouds I. *J. Atmos. Sci.,* **35,** 2111–2121.

——, 1980: Radiative properties of cirrus clouds in the infrared region. *J. Atmos. Sci.,* **37,** 435–445.

——, S. C. Tsay, P. W. Stackhouse, and P. J. Flatau, 1990: The relevance of the microphysical and radiative properties of cirrus clouds to climate and climatic feedback. *J. Atmos. Sci.,* **47,** 1742–1753.

Wiscombe, W., 1976: Extension of the doubling method to inhomogenous sources. *J. Quant. Spectrosc. Radiat. Transfer,* **16,** 477–489.

——, and G. W. Grams, 1976: The backscattered fraction in two-stream approximations. *J. Atmos. Sci.,* **33,** 2440–2451.

——, and J. W. Evans, 1977: Exponential-sum fitting of radiative transmission functions. *J. Comput. Phys.,* **24,** 416–444.

Wu, M. L. C., 1984: Radiative properties and emissivity parameterization of high level thin clouds. *J. Climate Appl. Meteor.,* **23,** 1138–1147.